Journal of Polymers and the Environment (2019) 27:1529–1541
https://doi.org/10.1007/s10924-019-01450-x

ORIGINAL PAPER

Nano Graphene-Reinforced Bio-nanocomposites Based on NR/PLA: The Morphological, Thermal and Rheological Perspective

Elnaz Esmizadeh[1] · Taha Sadeghi[2] · Ali Vahidifar[1,3] · Ghasem Naderi[2,4] · Mir Hamid Reza Ghoreishy[2] · Seyed Mohammad Reza Paran[2]

Published online: 23 April 2019

Abstract

Bio-based graphene-reinforced thermoplastic elastomers (TPE) based on natural rubber (NR), and poly lactic acid (PLA) were successfully prepared via melt blending. The effect of graphene nanosheets (GNS) content and coupling agent were investigated on morphological, thermal and rheological properties of the PLA/NR/GNS bio-nanocomposites. More stable morphology of uniformly dispersed NR phase in the continuous PLA matrix with a relatively narrower diameter-size distribution was achieved in the presence of a compatibilizer. Moreover, transmission electron micrographs showed more improved dispersion of GNS with predominantly exfoliated morphology in the case of ENR-compatibilized PLA/NR/GNS bio-nanocomposites. Crystallization/melting studies revealed that, as the GNS content increased, the cold-crystallization peak, melting peak and glass-to-rubber transition temperature values shifted to higher temperatures and the crystallinities of blends slightly decreased (about 7%) which might be attributed to the reduction of polymeric segments mobility by the restricting effect of GNS. Dynamical mechanical investigation showed that the storage modulus (E′) increased about 25% by the introduction of GNS due to the inherent stiffness of GNS and the occurrence of compatibility in the PLA/NR blend in the presence of ENR. The presence of ENR shifted the T_g of the NR phase and the PLA matrix towards each other which is a characteristic of higher miscibility and compatibility. The thermogravimetry (TGA) and derivative thermogravimetry (DTG) curves revealed higher thermal stability of the compatibilized-PLA/NR blends due to the enhanced interfacial adhesion and the homogenous dispersion of GNSs as direct effects of the presence of ENR. Rheological studies indicated that the formation of the effective GNS-polymer networks by the presence of ENR increased the storage modulus (G′) and complex viscosity (η^*) value due to the effectiveness of the GNS in taking loads and restricted molecular motion, respectively.

Graphical Abstract

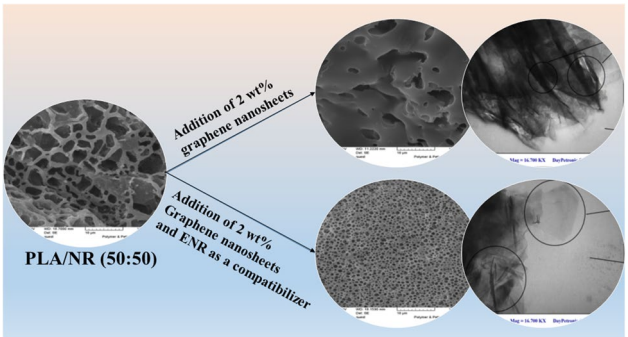

Keywords Nano graphene sheets · Bio-nanocomposites · Natural rubber · Poly lactic acid · Thermoplastic elastomer

✉ Ghasem Naderi
G.Naderi@ippi.ac.ir

Extended author information available on the last page of the article

Introduction

The increasing demands for new polymer materials in the market led to an extraordinary class of copolymers or polymer blend comprising an elastomeric polymer phase and a melt-processable plastic phase, known as thermoplastic elastomer (TPE), exhibiting elastomeric properties at room temperature, yet can be melt-processed like a typical thermoplastic [1–3]. TPEs pose less threat to the environment owing to several reasons as follows: (1) less-energy consumption during the process, (2) simple processing machines, (3) no need for further crosslinking like traditional rubbers, (4) the scraps generated during production are recyclable [4, 5]. However, the high level of concern for a clean and safe environment for the future has triggered spirited debate to find a new way to eliminate the extensive use of traditional rubber and plastic due to their unsustainability and environmental pollution. The use of bio-based polymers as sustainable alternatives to conventional petroleum-based rubbers and plastics paves the way to provide a promising solution to the address the above issues [6]. Generally, bio-based polymers, which have been received considerable attention in recent decades, are derived from renewable resources mainly including starch-based, cellulosic-based and soy-based polymers [7]. Bio-based polymers can express both biodegradable or non-biodegradable properties based on their chemical structure [8]. In this regard, poly (lactic acid) or PLA is one of the most promising biodegradable and biocompatible thermoplastics whose monomer is derived from the normal microbial fermentation process mainly from agricultural by-products of natural carbohydrates [4, 9, 10]. However, the inherent high brittleness and stiffness of PLA do not allow replacing commodity polymers in large scale for the applications where plastic deformation at high-stress levels is required [11]. To overcome these limitations, several approaches have been attempted to improve the toughness, flexibility, and ductility of PLA such as plasticization, blending, and copolymerization [6]. Among these methods, blending of PLA with rubbery polymers such as ethylene-co-vinyl acetate copolymer [12], nitrile butadiene rubber [13], natural rubber (NR) [8, 14, 15], polyester elastomer [16], ethylene-co-octane copolymer [17] and poly(ether-b-amide) [18, 19] as toughening agent is the most practical and the least expensive one [11]. The introduction of NR as the elastomer phase is of great interest because it not only enhances the flexibility and toughness of PLA, but also provides an entirely bio-based TPE since NR is perhaps the most abundant pioneer bio-polymer mainly derived from the Hevea Rubber tree [8, 14]. Moreover, although NR is not readily biodegradable, the presence of PLA can activate or accelerate biodegradation representing a tremendous technological advance in environmental concerns [8].

TPE bio-blend of PLA/NR and its nanocomposites have been studied by few researchers in the last decade, both experimentally and theoretically [8, 11, 20]. Jaratrotkamjorn et al. prepared rubber toughened PLA by blending with NR-based polymers via a twin screw extruder and studied the effect of the polarity, viscosity, mastication and molecular weight of NR on the properties of resultant TPEs [20]. They reported that NR is the best toughening agent than epoxidized-NR (ENR) and NR-grafted with poly methyl methacrylate (NR-g-PMMA), while the latter two provide higher miscibility to PLA than virgin NR [20]. A seven-fold increase in impact strength of PLA in the presence of 35 wt% of NR was reported by Xu et al. without any interfacial modification [21]. However, Glycidyl methacrylate-grafted NR (NR-g-GMA) was shown to be an effective compatibilizer for PLA/NR blend leading to better dispersion and distribution of NR in the PLA matrix and consequently a significant increase in toughness [22]. Pongtanayut et al. observed that NR or ENR rubber phase droplets could act as a nucleating agent and increased the crystallization ability of PLA in PLA/NR TPEs [11]. Also, the thermal stability of blends was found to be dropped with the addition of the both NR-based rubbers [11], while the hydrolysis rate and mechanism of PLA were not affected by NR, beneficial for keeping the biodegradability of PLA [23]. Tanrattanakul and coworkers confirmed that the solubility parameter and molecular weight of plasticizers are of crucial importance in controlling the mechanical properties and glass-to-rubber transition temperature of plasticized PLA/NR TPEs [8]. Chen et al. reported the formation of the continuous morphology for cross-linked NR phase instead of traditional sea-island morphology in PLA/NR blend after dynamic vulcanization of NR with various crosslinking systems including dicumyl peroxide, sulfur and phenolic resin curing system [24, 25]. This morphology was claimed to be quite novel in the field of dynamic vulcanization providing the excellent interfacial adhesion between the two polymer phases [24].

Recently, some findings have provided the proof that the addition of nanofillers including nano-SiO_2 [26], nanoclay [27], and cellulose nanowhisker [28, 29], into biopolymers to prepare bio-nanocomposites presents a practical way to improve the properties of PLA/NR bio blend. To the authors' best knowledge, literature, however, lacks data specifically on the properties of PLA/NR bio-polymers reinforced by graphene nanosheets (GNS). Hence, the authors approach here is to develop a novel and industrially scalable GNS-filled bio-nanocomposites based on PLA/NR bio-blend by melt blending. This study is aimed at understanding how influential is the reinforcing NGS on the mechanical, morphological and thermal response of PLA/NR TPE bio-blend.

Experimental

Materials

Poly lactic acid (PLA) with trade name of REVODE190 (L130) was purchased from Hisun® (China, Density: $\rho = 1.25 \pm 0.05$ g/cm^3, Melt Flow Index: MFI = 5–9 g/10 min). Natural Rubber (NR) SMR20 was kindly supplied by GM® (Malaysia, Mooney viscosity: ML(1 + 4)100 °C = 60 ± 5, $\rho = 0.91$ g/cm$^{3)}$. Graphene C-750 (surface area of 750 m^2/g, average thickness of 1-5 nm) was obtained from XG Science (USA). Epoxidized Natural Rubber (ENR) ENR50 (including 50 mol % of epoxidation), kindly provided by FELDA® Rubber Industries (Malaysia) was used as coupling agent or compatibilizer.

Preparation and Characterization

PLA and GNS were dried in a vacuum oven at 40 °C and 60 °C, respectively, for 12 h to remove the moisture prior to mixing. PLA/NR (blend ratio of 50:50) blends were prepared at different GNS contents with the presence of ENR as a compatibilizer. The sample codes for PLA/NR/GNS polymer bio-nanocomposites were defined according to the PLA/NR blend ratio, the presence of compatibilizer (2 phr), and GNS content, e.g., the PLA/NR blend samples reinforced by 2 phr of GNS were defined as P50/N50/E/G2 and P50/N50/G2 in the presence or absence of the compatibilizer (ENR), respectively. All ingredients were charged into the mixing chamber of internal mixer (HAKKE Rheomix 3000p, Germany) simultaneously at 180 °C and a rotor speed of 60 rpm for 6 min using high-intensity three-winged rotors. Subsequently, the blend was removed from the internal mixer and then compression molded into 1 mm thick sheets in a hot press at 210 °C under a pressure of 15 MPa.

The phase morphology of the fractured surface of PLA/NR blends was investigated with a scanning electron microscopy (SEM) imaging at 20 kV using XMU TESCAN-VEGA II microscope, Czech Republic. All samples were cryo-fractured in liquid nitrogen, and the fracture surface was sputter-coated with gold before the examination. Toluene etching at room temperature for 24 h was then be used to remove NR phase from the surface of the blend permanently, and consequently, the samples were kept in a vacuum oven for residual solvent removal. Number-average diameter $\left(D_n = \sum N_i D_i / \sum N_i\right)$, volume-average diameter $\left(D_v = \sum N_i D_i^4 / \sum N_i D_i^3\right)$ and polydispersity index ($PDI = D_v/D_n$) were determined by measuring the diameters of at least 60 droplets using the ImageJ software. The dispersion state of GNSs in the polymer matrix was more precisely investigated by Transmission electron microscopy (TEM) test using an EM2085 microscope (Philips, Netherland) operating at 120 kV. Ultrathin sections of the samples were cut using an OMV reichert ultra-microtome (Austria) equipped by a diatome diamond knife.

Crystallization and melting behavior of the PLA/NR/GNS bio-nanocomposites were investigated in three steps by DSC200F3 (Netzsch Instruments, Germany) at nitrogen atmosphere. Samples of about 5–10 mg were loaded into a DSC apparatus after precise weighing and sealing in aluminum pans. Firstly, the samples were heated from 25 to 210 °C at a heating rate of 10 °C/min and were kept for 3 min at 210 °C to remove any residual thermal history and small nuclei that might act as seed crystals. Then, the samples were cooled to 25 °C at a cooling rate of 10 °C/min, cooling scan, to study cold crystallization behavior. In the end, they were heated again to 210 °C at the same rate of heating, heating scan, to study their melting behavior. In this test, the glass transition temperature (T_g), cold crystallization temperature (T_{cc}), melting temperature (T_m) and degree of crystallization (x_c) of PLA/NR/GNS bio-nanocomposites were determined. The degree of crystallization or crystallinity (χ_c) of PLA50/NR50 nanocomposites, was assessed in accordance with the below Eq. (1):

$$x_c(\%) = \frac{\Delta H_m - \Delta H_c}{\Delta H_m^o \times W_f} \times 100 \quad (1)$$

where ΔH_m is the enthalpy of melting, ΔH_m^0 is the enthalpy of melting of 100% crystalline PLA, W_f is weight fraction of PLA in blends and ΔH_c is enthalpy of crystallization of PLA.

Dynamic mechanical analysis (DMA) was performed on a 2000DMATitec (Triton Technology, England) and viscoelastic properties of PLA/NR blends such as storage modulus (G'), loss modulus (G'') and damping factor (tan δ) were measured as a function of temperature. The test was conducted in the temperature range of -100 to 150 °C at a heating rate of 5 °C/min on compression-molded rectangular bars having dimensions of 3 cm × 2 cm × 1 mm size.

Thermal stability of PLA/NR/GNS nanocomposites was investigated using thermogravimetric analysis (TGA) instrument (PL-150, Mettler Toledo, Switzerland) at a heating rate of 10 °C/min in the temperature range of 25 to 600 °C under nitrogen atmosphere. The onset temperature of degradation ($T_{onset,deg}$) and the degradation temperature ($T_{peak,deg}$) was measured from the 5% of weight loss and maximum weight loss rate temperature, respectively.

Rheological measurements were performed using a parallel plate rheometer (Physica MCR501, Anton Paar, Austria) with geometry of 25 mm of diameter fixture at 210 °C. The melt rheological properties were studied using a strain

controlled (1%) in frequency sweep mode from 0.01 to 600 rad/s frequency range under an inert nitrogen atmosphere in order to prevent oxidative degradation of polymers.

Results and Discussion

Morphological Investigation

In order to probe the effect of compatibilizer and GNS on the phase morphology of PLA/NR/GNS bio-nanocomposites, morphological investigations were accomplished using SEM and TEM. Figure 1 shows an SEM micrograph of a cryo-fracture surface of the 50/50 PLA/NR bio-blend containing various amount of GNS and the extracted data including number-average (D_n) and volume-average (D_v) diameters of the dispersed phase (NR) are given in Table 1. As a first appreciation, these results reveal significant reductions in the particle size of the dispersed phase (NR) in the presence of GNS and compatibilizer. The D_n and D_v of the NR phase in the unfilled un-compatibilized blend (P50/N50) are found to be 3.41 μm and 8.66 μm, respectively. Moreover, its morphology is unstable towards

Table 1 Number-average (D_n) and volume-average (D_v) diameter of NR phase in PLA/NR/GNS bio-nanocomposites

Sample	$D_n = \frac{\sum N_i D_i}{\sum N_i}$	$D_v = \frac{\sum N_i D_i^4}{\sum N_i D_i^3}$	$PDI = \frac{D_v}{D_n}$
P50/N50	3.41	8.66	2.53
P50/N50/E/G0.5	2.49	4.17	1.67
P50/N50/E/G1	1.69	2.04	1.20
P50/N50/E/G1.5	0.94	1.10	1.16
P50/N50/E/G2	0.62	0.74	1.19
P50/N50/G2	3.08	10.02	3.31

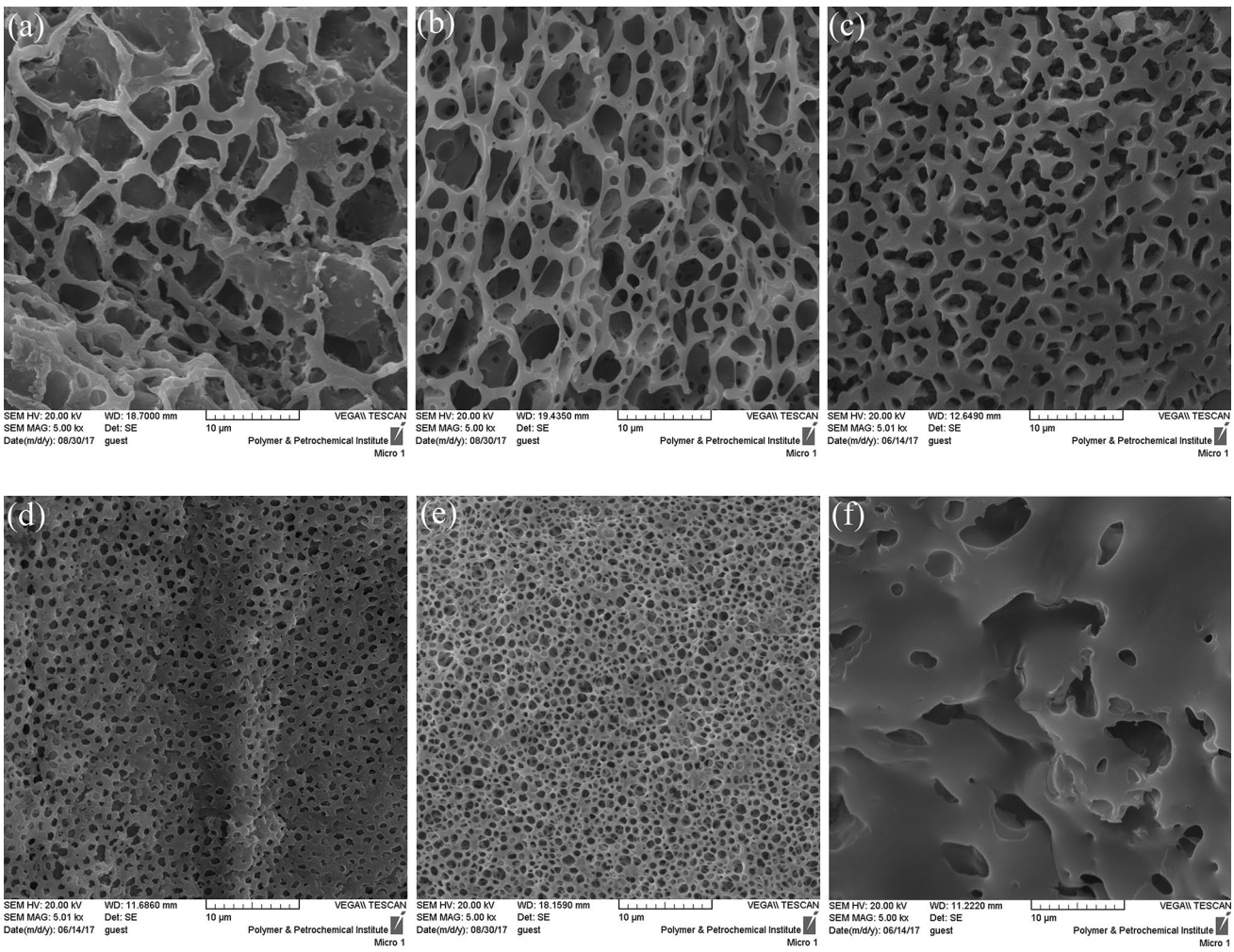

Fig. 1 Phase morphology and distribution of rubber droplet size in PLA/NR/GNS bio-nanocomposites blends at different GNS content: **a** P50/N50, **b** P50/N50/E/G0.5, **c** P50/N50/E/G1, **d** P50/N50/E/G1.5, **e** P50/N50/E/G2; P50/N50/G2

coalescence during melt processing which consequently forms a coarse morphology, consisting of both un-shaped PA6 particles.

On the other hand, the D_n and D_v of the NR phase in the compatibilized blend (P50/N50) filled with 2 wt% of GNS (P50/N50/E/G2) are decreased to 0.62 µm and 0.74 µm, respectively. There is also evidence of more stable morphology with a relatively narrower diameter-size distribution (when PDI approaches unity, PDI → 1) of predominantly spherical or slightly elongated shape NR phase in this system. The literature on polymer blend phase morphology have revealed that the viscosity ratio of a blend is substantially influential in the determination of the final size of the dispersed phase which is controlled by the competition between the coalescence and breakup phenomena [30]. A higher viscosity ratio of a blend contributes to droplets of a larger size for the dispersed phase [31, 32]. The addition of GNS enhances the viscosity of the elastomeric phase, suggesting that the viscosity difference between two phases becomes negligible and as a result, the viscosity ratio of the blend would be expected to be approaching to unity [33].

Moreover, it has been verified that besides the viscosity ratio of the blend, interfacial tension plays a crucial role in the determination of the dispersed phase droplet size [31]. As evidenced from the SEM micrographs of compatibilized and uncompatibilized PLA/NR blends with 2 wt% of GNS (P50/N50/E/G2 and P50/N50/G2, Fig. 1e and f, respectively), the presence of the compatibilizer (ENR) decreases the size of the dispersed NR domains. This is due to the ability of the compatibilizer to suppress the coalescence of the droplets which as a consequence reduces the droplet size significantly. This indicates that ENR which as a compatibilizer locates at the interface of the two phases should be very efficient in lowering the interfacial tension and stabilizing the morphology against coalescence. It is shown that the main advantage of using compatibilizers in polymer blends is to form a robust interfacial adhesion to achieve a good stress transfer across the interface and a significant reduction in the dispersed phase domain size [34]. Based on the SEM micrographs, it can be concluded that the domain size of the dispersed phase is altered by the change in deformability originating from the variation of the viscosity ratio of the blend as well as the interfacial tension.

In order to gain a further understanding where the GNSs were located in the blend and how well they were dispersed into the PLA/NR blend, TEM investigation was accomplished. Figure 2 shows the TEM micrograph of the compatibilized and un-compatibilized PLA/NR blend reinforced by 2 wt % of GNS, P50/N50/E/G2 and P50/N50/G2, respectively. Light regions depict the phase with lower density (NR, 0.91 g/cm^3) and darker regions are representatives of the denser phase (PLA, 1.25 g/cm^3); the black lines are related to the cross-section of GNS with the density of 2.25 g/cm^3 dispersed within the matrix [30]. TEM observation unveiled that all the GNSs are selectively located in the NR phase or their interface. The dispersion state of GNSs in the PLA/NR blend is found to be strongly dependent on the presence of the compatibilizer. Figure 2a displays that GNSs are exfoliated into thin tactoids that contain only a few graphene sheets dispersing uniformly and randomly in the PLA/NR matrix. This indicates that the presence of compatibilizer is effective to promote both the exfoliation (ultra-thin CNS tactoids of the thickness of ~ 2–5 nm) and intercalation of GNS (thin CNS tactoids of the thickness of ~ 10–20 nm).

In contrast, without the addition of any compatibilizer (P50/N50/G2), large agglomerates or thick tactoids of GNS (over some hundreds of nanometers of thickness) are also observed (Fig. 2b). This further corroborated the compatibilizing effect of ENR at dispersing GNS in PLA/NR bioblend. The leading reason behind nano-sheets separation, particularly exfoliation, is the establishment of favorable interactions between the polymer and the GNS surface and the subsequent drop in energy of the system [35]. Achieving exfoliated morphology for layered nano-fillers gives rise to composite materials with a wide range of enhanced performance, such as mechanical, thermal and gas barrier properties, at the same nano-filler loading [36].

Crystallization and Melting Properties

The objectives of DSC experiments were to investigate the effect of GNS and coupling agent on melting and crystallization behavior of the PLA/NR TPE blends whether or not any change in the glass transition temperature (T_g) occurred.

Figure 3 shows the DSC cooling thermograms of PLA/NR/GNS nanocomposites with different GNS content. Neat

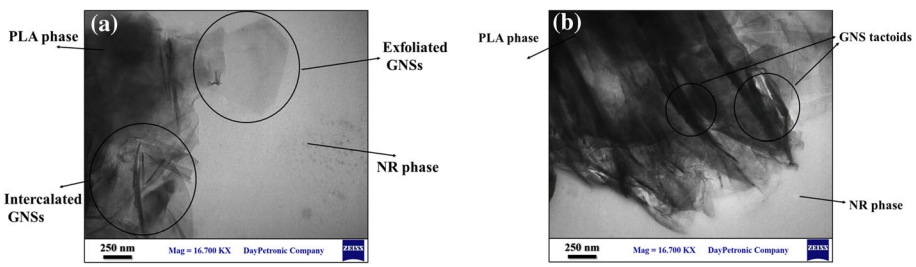

Fig. 2 TEM micrograph of compatibilized PLA/NR/GNS bio-nanocomposite containing 2 wt% of GNS (P50/N50/E/G2)

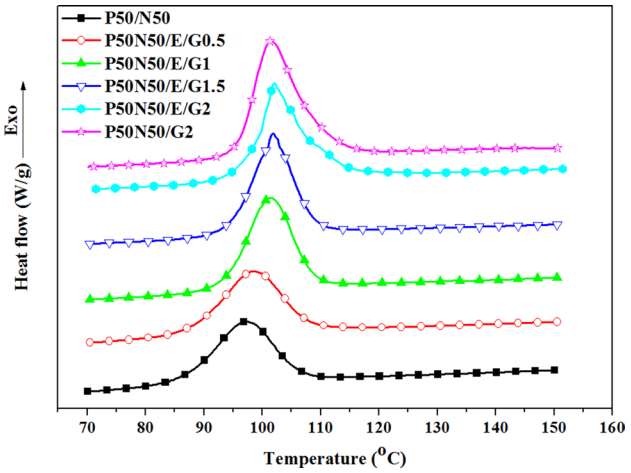

Fig. 3 DSC thermograms of PLA/NR/GNS nanocomposites with various contents of GNS obtained from first cooling scan

PLA/NR blend and its related nanocomposites exhibit a similar trend in thermograms showing a sharp PLA-derived cold-crystallization exothermic peak at about 100 °C.

A summary of the thermal characteristics including enthalpy of cold-crystallization, the crystallization initiation temperature, the cold-crystallization peak temperature, temperature range of crystallization and crystallization time obtained from the cooling scan of DSC curves are tabulated in Table 2. The table reveals that in the case of PLA/NR with dispersed GNS, the cold-crystallization peak values shifted to higher temperatures proportional to the respective GNS concentrations, while the crystallinities of blends slightly decreased with increasing GNS content. Dispersion state of GNS in the matrix was found to be influential in governing crystallization initiation, growth, and final crystallinity level of a polymer matrix. The more improved dispersion of GNS in the polymer matrix, the more efficient crystallization nucleation, and lower crystallization initiation temperature, i.e. quicker crystallization [11, 37].

Moreover, reduced chain mobility of crystallable polymer (PLA here) due to the formation of strong GNS–polymer interactions and the presence of GNS favors the reduction in crystallinity of the polymers [38]. In comparison, at the same content of GNS (2 phr), the cold-crystallization peak of the crystallable phase shifted to the higher temperature in the presence of ENR, as seen in Table 2. It should contribute to the good interfacial compatibility between PLA and NR phases probably occurred via chemical interaction between the oxirane ring on ENR with the hydroxyl groups of PLA [11], as well as the improved GNS dispersion state (will be shown in morphology section).

DSC thermograms of PLA/NR/GNS bio-nanocomposites during the second heating scan is demonstrated in Fig. 4. The blends with higher content of GNS exhibited a melting peak, and glass-to-rubber transition temperature at higher temperatures which might be ascribed to the reduction of polymeric segments mobility by the restricting effect of GNS and in consequence increased stiffness of the polymer matrix [39]. Compared with the un-compatibilized PLA/NR/G2, ENR-compatibilized sample (PLA/NR/E/G2) demonstrated an increment in the abovementioned values.

Table 2 Crystallization melting characteristics of PLA/NR/GNS nanocomposites from first cooling and second heating cycles of DSC

Samples	Enthalpy of crystallization (E_{cry}, J/g)	Onset temperature of crystallization ($T_{onset,cry}$, °C)	Peak temperature of crystallization ($T_{peak,cry}$, °C)	Temperature range of crystallization (°C)	Time of crystallization (t_{cry}, s)
First cooling cycle					
P50/N50	14.24	106.8	97.5	19.7	118.7
P50/N50/E/G0.5	14.12	107.9	98.6	19.0	116.1
P50/N50/E/G1	13.51	108.8	101.4	15.0	114.9
P50/N50/E/G1/5	113.43	108.9	101.9	14.3	113.6
P50/N50/E/G2	14.21	109.2	102.2	12.1	111.8
P50/N50/G2	16.28	107.7	101.6	15.2	114.1

Samples	Enthalpy of melt (E_{melt}, J/g)	Onset temperature of melt ($T_{onset,melt}$, °C)	Peak temperature of melt ($T_{peak,melt}$, °C)	Crystallization degree (s)*
Second heating cycle				
P50/N50	24.97	166.3	173.9	25.7
P50/N50/E/G0.5	23.99	166.5	174.2	25.2
P50/N50/E/G1	22.44	167.4	174.7	24.7
P50/N50/E/G1.5	21.61	168.0	175.1	24.0
P50/N50/E/G2	21.1	168.3	175.4	23.6
P50/N50/G2	23.43	166.9	174.9	23.9

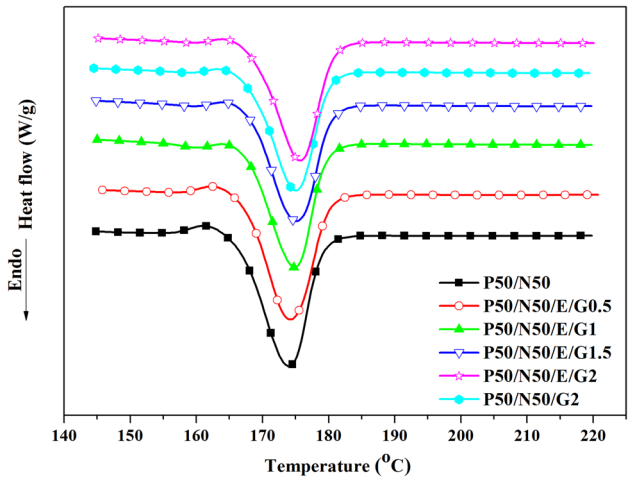

Fig. 4 DSC thermograms of PLA/NR/GNS nanocomposites with various contents of GNS obtained from second heating scan

This implies that, once the interfacial interaction between PLA and NR enhances thanks to the chemical reactions, the segmental motions of polymeric chains will be further restricted [40].

Dynamic Mechanical Analysis

To further understand the effect of GNS and compatibilizer on dynamical-mechanical properties, viscoelastic, damping behavior, and molecular interaction of polymeric phases, DMTA was performed on the prepared PLA/NR/GNS bio-nanocomposite samples. Figure 5 shows the variation of dynamic elastic or storage modulus (E′) of PLA/NR (50:50) TPE blend and its GNS-reinforced nanocomposites, over the temperature range from − 90 to 90 °C.

It is seen that the initial E′ of PLA/NR/GNS bio-nanocomposite samples within the glass region at temperatures below − 60 °C was increased by the use of GNS due to the intrinsic stiffness of GNS. The occurrence of compatibility in the PLA/NR blend in the presence of ENR as the compatibilizer induced by some molecular interaction between PLA and NR chains may also be taken into account in the

Fig. 5 Temperature dependence of storage modulus (E′) in PLA/NR/GNS nanocomposites

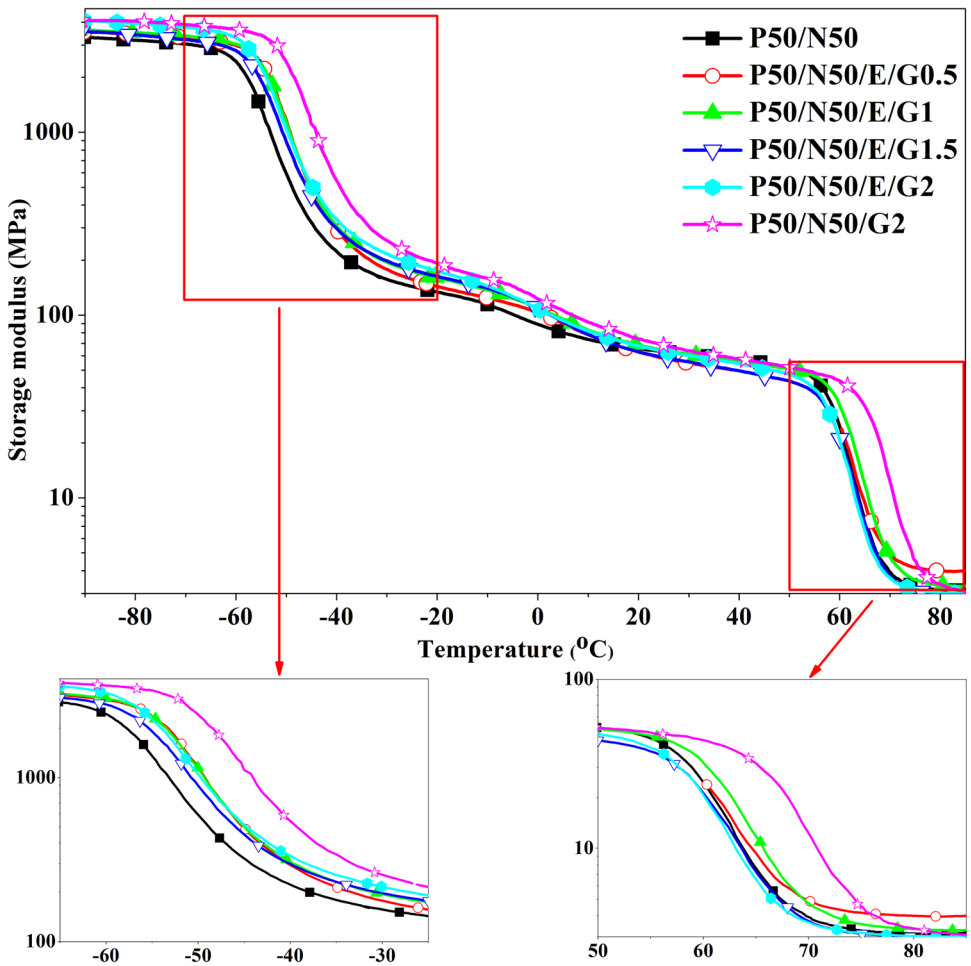

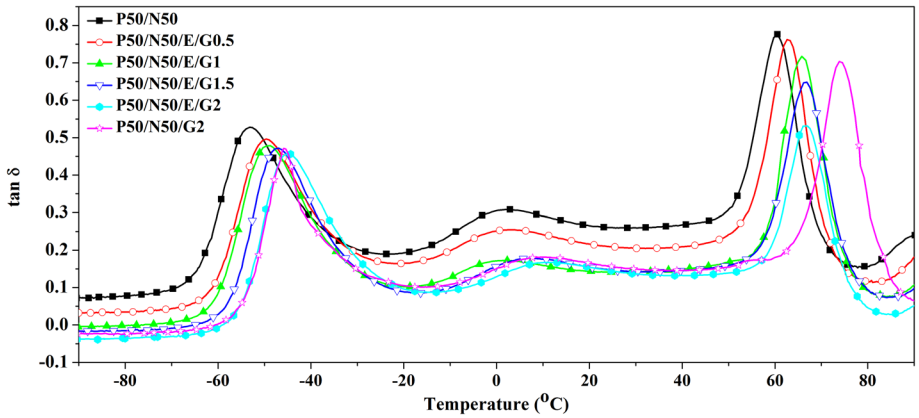

Fig. 6 Temperature dependence of loss factor (tan δ) in PLA/NR/GNS nanocomposites

E′ enhancement [41]. The E′ curve of all samples exhibits two significant sharp drops corresponding to the glass transition temperatures of their two polymeric constituents, PLA phase and NR phase. These two distinctive drops in the E′ curves imply the presence of two differentiable phases in the samples revealing the immiscibility of the system [41].

Figure 6 exemplifies the temperature dependence of the loss factor $\left(\tan = \frac{E''}{E'}\right)$. The temperatures of the two peaks in tan curves illustrate two remarkable α-transition temperatures equivalent to the T_g of the polymeric phases (tabulated in Table 3). It is found that the temperatures of the peaks in PLA/NR/GNS bio-nanocomposites upturns with increasing GNS content. For instance, the T_g of the NR phase (−53.22 °C) in the PLA/NR/E/G0.5 bio-nanocomposite is slightly higher than that of NR in PLA/NR blend (−49.66 °C), and with adding more GNS, it further increases. The same argument applies to the variation of the T_g of the PLA phase with increasing GNS amount, which may be attributed to the rise in restriction of segmental motion of PLA and NR polymeric chains in the presence of GNS. The height of the tan peak provides information about damping characteristics and the dissipated mechanical energy in the sample. The figure shows that the height of the tan peaks for NR and PLA in nanocomposite samples are lower than that of neat PLA/NA blend and it gradually decreases with an increase in GNS loading. This is also indication of the hindered polymeric segmental mobility caused by the presence of GNS as discussed above.

It is worth mentioning that at the same GNS content (here 2 phr of GNS), the presence of ENR causes the T_g of the NR phase and that of the PLA matrix shift towards each other. This observation substantiated a characteristic of higher miscibility and the influence of ENR on improving compatibility of PLA and NR due to some molecular interaction between them, confirmed by Nematollahi et al. [41]. In other words, ENR graft copolymer acts as a compatibilizer and promotes interfacial adhesion between the PLA and NR. Moreover, the broader tan peak or higher peak width is indication of the interaction between phases. Relatively higher peak width of P50/N50/E/G2 sample in comparison with that of P50/N50/G2 once again confirms the above explanations which imply higher interaction and lower interfacial tension between PLA and NR chains in the presence of ENR.

Thermal Stability

The thermal stability of GNS-reinforced PLA/NR bio-nanocomposites was determined by thermogravimetric analysis (thermograms are shown in Fig. 7). The first derivative of TGA curves (DTG) obtained using TA analysis software is given in Fig. 8. The TGA weight loss curves

Table 3 The glass transition temperature of two polymeric phases and initial storage modulus of PLA/NR/GNS bio-nanocomposites determined by DMA

Samples	NR glass-to-rubber transition temperature (T_g, °C)	tan δ intensity of first peak	PLA glass-to-rubber transition temperature (T_g, °C)	tan δ intensity of second peak	Initial storage modulus (E'_{ini}, *MPa*)
P50/N50	−53.22	0.52	60.54	0.77	3283
P50/N50/E/G0.5	−49.66	0.49	62.63	0.76	3544
P50/N50/E/G1	−48.72	0.47	65.77	0.71	3556
P50/N50/E/G1/5	−47.10	0.47	66.86	0.64	3602
P50/N50/E/G2	−44.33	0.45	66.95	0.53	4049
P50/N50/G2	−45.84	0.47	73.83	0.70	4055

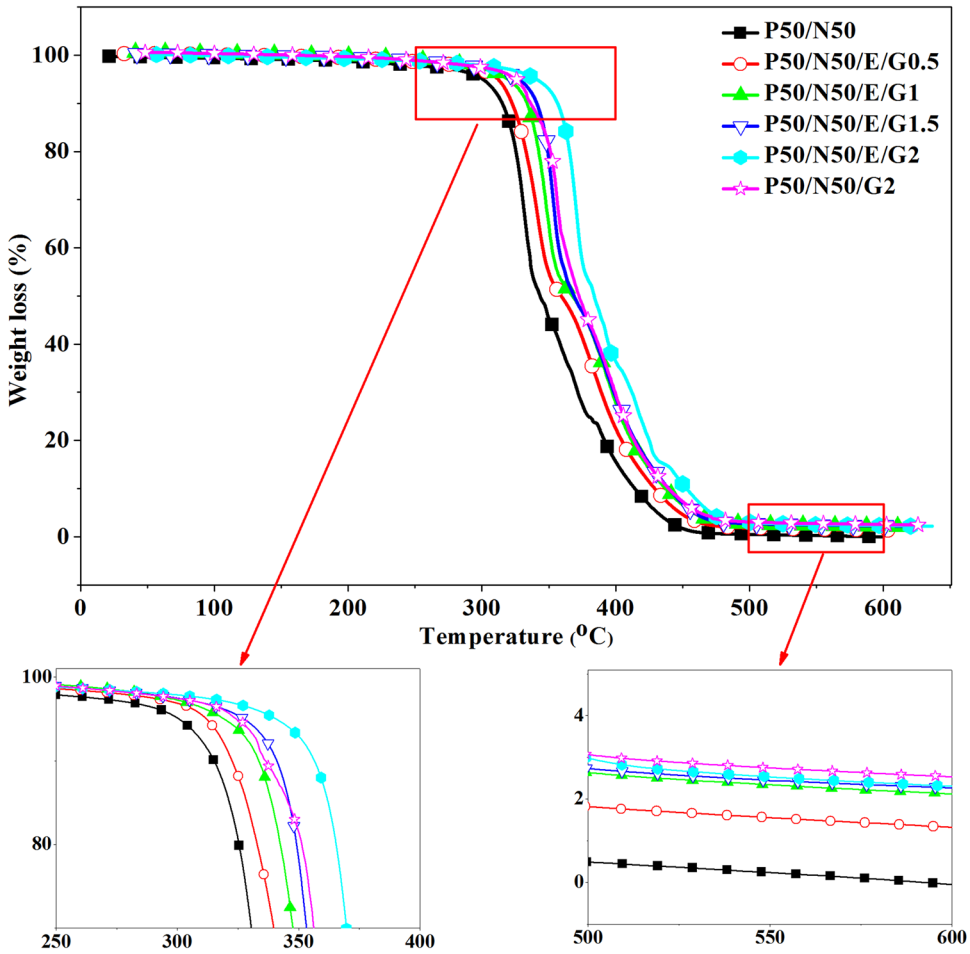

Fig. 7 TGA thermograms of graphene-reinforced PLA/NR bio-nanocomposites

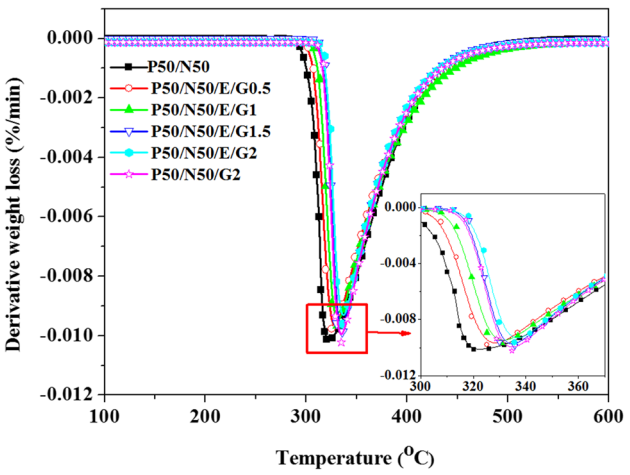

Fig. 8 DTG curves of graphene-reinforced PLA/NR bio-nanocomposites

of PLA/NR/NGS bio-nanocomposites display a typical sigmoidal shape, and their first derivatives display only one peak regardless the effect of graphene, which both are shreds of evidence of the occurrence of single step weight loss in 250–400 °C range.

The thermal degradation characteristic values including the 5% weight loss temperature (onset temperature of degradation, $T_{onset,deg}$) and fastest decomposition temperature (peak temperature of degradation, T_{deg}) of the samples calculated from the above thermograms are tabulated in Table 4.

Analysis of the decomposition behavior of PLA/NR/GNS bio-nanocomposites discloses that the thermal decomposition of virgin PLA/NR blend initiates at 291.3 °C, then it reaches to its fastest degradation rate, ascribed to the maximum peak position of the first derivative curve, at 320.9 °C. In the presence of the graphene nano-pellets, the degradation onset temperature, along with the peak degradation temperature, shift into a high temperature, about several degrees higher than that of the virgin PLA/NR blend. For instance, compared with the virgin blend, the $T_{onset,deg}$, and $T_{peak,deg}$ of the P50/N50/E/G0.5 blend (the sample with just 0.5 wt% of GNS) is slightly increased to 295.4 °C and 336.4 °C, respectively, showing 4.1 °C and 5.5 °C increase, respectively. The enhancement effect of GNS on thermal stability of the PLA/NR bio-blend is more pronounced in the high loading of it. Based on the above descriptions, it can be concluded that the

Table 4 Thermal degradation properties of graphene-reinforced PLA/NR bio-nanocomposites

Sample	Onset temperature of degradation ($T_{onset,\deg}$, °C	Peak temperature of degradation ($T_{peak,\deg}$, °C	Residual ash (%)
P50/N50	291.3	320.9	0.14
P50/N50/E/G0.5	295.4	326.4	1.47
P50/N50/E/G1	300.7	330.2	2.26
P50/N50/E/G1/5	312.6	334.1	2.44
P50/N50/E/G2	314.3	336.2	2.54
P50/N50/G2	312.8	335.6	2.57

GNS can improve the thermal stability of virgin PLA/NR blend by hindering the thermal decomposition process. This agrees with the well-established theory that intercalated/exfoliated nanosheets provide physical hindrance against the diffusion of small volatile decomposition products which consequently retards thermal degradation phenomenon. This was due to that the well-dispersed nanosheets contribute to a high-tortuosity path which reduces the molecular mobility and thereby retarding the diffusion of the small gaseous molecules [42].

It is found from Table 4 that the PLA/NR/GNS bio-nanocomposite in the presence of the compatibilizer exhibits a substantially higher thermal stability compared with the sample without the compatibilizer. In the case of PLA/NR blend containing 2 wt% of GNS, the sample with compatibilizer, P50/N50/E/G2, shows comparatively higher thermal stability in comparison with the sample without the compatibilizer, P50/N50/G2. This difference might be accredited to the improved interaction between the polymeric components leading to better dispersion of GNS in polymer matrix induced by the presence of the compatibilizer. This result is entirely in concordance with the morphological observation, which exhibits enhanced intercalated/exfoliated dispersion state of GNS in the presence of ENR as the compatibilizer. Improved thermal stability of the blends due to the greater interfacial adhesion between the blend components and the homogenous dispersion of nanomaterials as direct effects of the presence compatibilizing agent have also been reported in the literature [22]. Better dispersion of the GNSs in PLA/NR blend, the higher the thermal stability of the resultant nanocomposites. Owing to the higher particle–polymer interaction resulted from a better dispersion of the GNSs in compatibilized PLA/NR/GNS bio-nanocomposites, these materials have a markedly limited segmental mobility in polymeric chains. Therefore, the barrier effect of GNS hindering the diffusion of the volatile decomposition products is much more pronounced with better dispersion of GNS and consequently results in higher thermal stability [13]. TGA also substantiates that there is a tremendous increment in the residual ash (char residue) with increasing the concentration of GNSs, which reflects the fact that they act as a thermal barrier and thereby affirming the observed improvement in thermal stability. Moreover, due to the high thermal stability of GNSs, they can successfully withstand degradation at high temperatures and remain as residue [43, 44].

Rheological Properties

Not only is the rheological characterization a sensitive method to reveal the overall dispersion state of GNS in polymer matrix besides the morphological technique of TEM, but it also is of crucial importance to understand the processability of materials. Figure 9 shows the rheological behavior of PLA/NR/GNS bio-nanocomposites, i.e., $\eta * \propto \omega$ and $G' \propto \omega$. It is observed in Fig. 9a that $\eta *$ decreases with frequency for both virgin and GNS-filled PLA/NR bio-blend, indicative of non-Newtonian pseudoplastic behavior. This means that no significant change is observed in the global trend of $\eta *$ versus frequency (pseudoplastic behavior) when GNS is added to the PLA/NR bio-blend. Such solid-like behavior observed in the nanocomposite samples could be attributed to the formation of a tridimensional network of well-dispersed GNS and also the neighboring dispersed phase droplets as compatibilizer suppresses the coalescence due to improved interface [27]. Despite the similar trend of $\eta *$ in all PLA/NR/GNS samples, the absolute value of the complex viscosity increases with increasing the concentration of GNS and the presence of compatibilizer in the whole range of the frequency. For example, the complex viscosity of PLA/NR blend increases by about 60% when 2 wt% of GNS is added into the blend in the presence of compatibilizer (P50/N50/E/G2). It can be attributed to the increased mixing viscosity due to the intrinsic stiffness and rigidity of GNS as well as improved interaction between GNS and polymer matrix, induced by the compatibilizing function of ENR. Such change the interfacial tension results in the coalescence suppression of the droplets which effectively reduces the dispersed phase droplet size (as observed in morphological section).

The evolution of storage modulus (G′) with frequency for PLA/NR bio-blend with various content of GNS, is illustrated in Fig. 9b. As can be seen, for all the bio-nanocomposite samples, the G′ indicates a gradual increase with frequency. At low frequencies, at the molecular level,

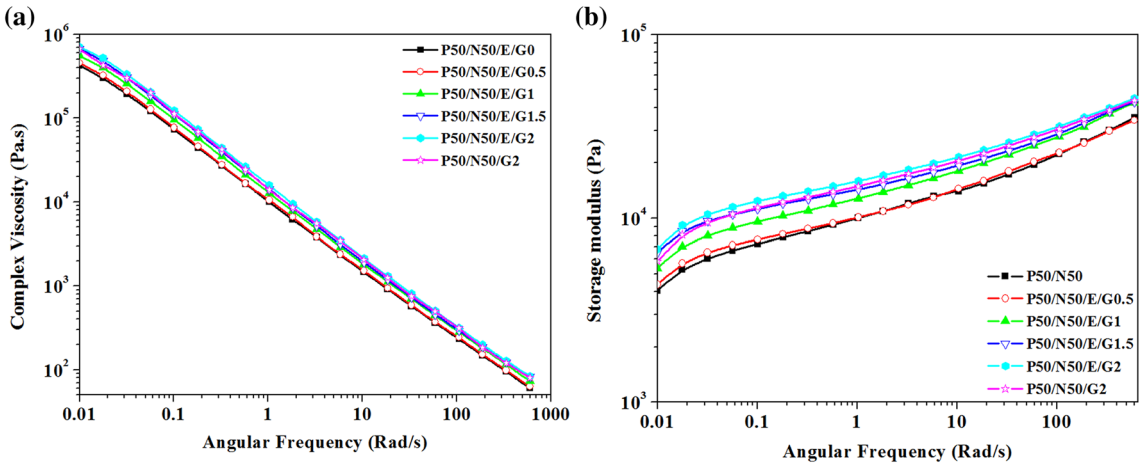

Fig. 9 Influence of GNS concentration and compatibilizer on rheological properties of PLA/NR/GNS bio-nanocomposites: variation of **a** complex viscosity and **b** storage modulus as a function of the angular frequency

the polymer segments get sufficient time to relax and, as a result, low values of storage modulus are witnessed. While, at higher frequencies, polymer molecules do not get enough time to allow the relaxation process due to the rapid deformation, and hence high values of storage modulus are observed [45].

The storage modulus rises gradually with higher GNS content; the sample P50/N50/E/G2 shows the highest G′ at all frequencies. This enhancement may be credited to the resistance to deformation of the polymer chains and the formation of strong GNS–polymer interactions, imposed by the presence of higher GNS content. Another reason can be the improved compatibility between the two polymers and the increase in the dispersion state of the GNS in the polymer matrix, imposed by the presence of the compatibilizer. It is worth noting that these effects are more pronounced at a low frequency confirming the solid-like behavior observed in the blend due to the formation of a tridimensional network [46]. On the other hand, the effect of GNS on the enhancement of storage modulus becomes nonsignificant at the high-frequency region which may suggest a restricted relaxation phenomenon at high frequencies. It is also interesting to see that the frequency-dependence of G′ in PLA/NR/GNS bio-nanocomposites is dependent on GNS content. Apparently, the dependence of storage modulus on frequency becomes weak with increasing GNS loading.

The effect of compatibilizer on the storage modulus of the PLA/NR/GNS bio-nanocomposites can be investigated by comparing the figures of P50/N50/E/G2 and P50/N50/G2. The storage modulus of the compatibilized sample is slightly higher that of the composite without the compatibilizer, as is evident from Fig. 9b. Uniform dispersion of GNS in the polymer matrix is achieved with the assistance of compatibilizer, as it is discussed in the morphological study section. Thus, the formation of the effective GNS-polymer networks by the presence of compatibilizer restricts the molecular motion, which thereby increases the storage modulus value.

Conclusion

The addition of natural rubber (NR) and GNS to Poly (lactic acid) PLA matrix allowed a straightforward production of toughened bio-nanocomposites with tunable properties by melt blending. The morphological, thermal and rheological properties were shown to be controlled as a function of the GNS content and the presence of the compatibilizer. From the results attained in this study, the following conclusions could be achieved:

- The phase morphology results indicated that the diameter of NR particles dispersed in the PLA matrix decreased with increasing GNS content and the presence of compatibilizer stemming from the improved compound viscosity and increased interfacial area. More stable morphology with a comparatively narrower diameter-size distribution of predominantly spherical shape was achieved for NR phase in compatibilized PLA/NR/GNS system.
- TEM observation revealed that compatibilized PLA/NR/GNS displayed that GNSs were exfoliated into thin tactoids containing only a few uniformly-dispersed graphene sheets, whereas large agglomerations of GNS were witnessed without compatibilizer.
- DSC cooling thermograms showed that the crystallization peak values shifted to higher temperatures and the crystallinities of blends slightly decreased with increasing GNS content and the presence of compatibilizer, due to the improved interfacial compatibility and improved

GNS dispersion state. The heating scan illustrated that the ENR-compatibilized sample displayed a significant increment in melting peak and glass-to-rubber transition temperature compared with the un-compatibilized PLA/NR sample.

– The DMTA results showed higher storage modulus (E′) and lower loss factor $\left(\tan = \frac{E''}{E'}\right)$)with increasing GNS loading due to the inherent stiffness of GNS. Relatively the broader tan peak thanks to the higher interaction between phases and lower interfacial tension between PLA and NR chains was observed in the presence of ENR as the compatibilizer
– It can be concluded form TGA/DTG curves that well-dispersed GNS contributed to a high-tortuosity path reducing the molecular mobility, and thereby increasing the thermal stability of PLA/NR bio-blend.
– Rheological observations showed that the storage modulus and complex viscosity rose with higher GNS content and the presence of the compatibilizer which can be credited to the resistance to deformation of the polymer chains and the formation of strong GNS–polymer interactions and the formation of a tridimensional network of well-dispersed GNS.

References

1. Esmizadeh E, Naderi G, Ghoreishy Mir Hamid R, Bakhshandeh Gholam R (2011) J Polym Mater 31:83
2. Esmizadeh E, Irani A, Naderi G, Ghoreishy MHR, Dobious C (2018) J Appl Polym Sci 135:45977
3. Vahidifar A, Esmizadeh E, Elahi M, Ghoreishy MHR, Naderi G, Rodrigue D (2019) J Appl Polym Sci 136:47795
4. Kang H, Hu X, Li M, Zhang L, Wu Y, Ning N, Tian M (2015) RSC Adv 5:23498
5. Delkash M, Naderi G, Sahraieyan R, Esmizadeh E (2017) Sci Eng Compos Mater 24:669
6. Ma P, Xu P, Liu W, Zhai Y, Dong W, Zhang Y, Chen M (2015) RSC Adv 5:15962
7. Fu Y, Liu L, Zhang J (2014) ACS Appl Mater Interfaces 6:14069
8. Tanrattanakul V, Bunkaew P (2014) Express Polym Lett 8:387
9. Karim MN, Rigout M, Yeates SG, Carr C (2014) Dyes Pigment 103:168
10. Karim MN, Afroj S, Rigout M, Yeates SG, Carr C (2015) J Mater Sci 50:4576
11. Pongtanayut K, Thongpin C, Santawitee O (2013) Energy Procedia. 34:888
12. Ma P, Hristova-Bogaerds D, Goossens J, Spoelstra A, Zhang Y, Lemstra P (2012) Eur Polym J 48:146
13. Talbamrung T, Kasemsook C, Sangtean W, Wachirahuttapong S, Thongpin C (2016) Energy Procedia. 89:274
14. Tanrattanakul V, Bunkaew P, Boonlong N (2012) J Biobased Mater Bioenergy 6:573
15. Bitinis N, Verdejo R, Cassagnau P, Lopez-Manchado M (2011) Mater Chem Phys 129:823
16. Zaman HU, Song JC, Park L-S, Kang I-K, Park S-Y, Kwak G, Park B-S, Yoon K-B (2011) Polym Bull 67:187
17. Moura I, Botelho G, Machado A (2014) J Polym Environ 22:148
18. Zhang W, Chen L, Zhang Y (2009) Polymer 50:1311
19. Han L, Han C, Dong L (2013) Polym Int 62:295
20. Jaratrotkamjorn R, Khaokong C, Tanrattanakul V (2012) J Appl Polym Sci 124:5027
21. Xu C, Yuan D, Fu L, Chen Y (2014) Polym Test 37:94
22. Juntuek P, Ruksakulpiwat C, Chumsamrong P, Ruksakulpiwat Y (2012) J Appl Polym Sci 125:745
23. Huang Y, Zhang C, Pan Y, Zhou Y, Jiang L, Dan Y (2013) Polym Degrad Stab 98:943
24. Chen Y, Yuan D, Xu C (2014) ACS Appl Mater Interfaces 6:3811
25. Yuan D, Chen K, Xu C, Chen Z, Chen Y (2014) Carbohyd Polym 113:438
26. Liu Y, Cao L, Yuan D, Chen Y (2018) Compos Sci Technol 165:231
27. Bitinis N, Verdejo R, Maya E, Espuche E, Cassagnau P, Lopez-Manchado M (2012) Compos Sci Technol 72:305
28. Bitinis N, Verdejo R, Bras J, Fortunati E, Kenny JM, Torre L, López-Manchado MA (2013) Carbohyd Polym 96:611
29. Bitinis N, Fortunati E, Verdejo R, Bras J, Kenny JM, Torre L, López-Manchado MA (2013) Carbohyd Polym 96:621
30. Razavi-Nouri M, Karami M, Naderi G (2017) Appl Clay Sci 145:1
31. Abdolrasouli MH, Behzadfar E, Nazockdast H, Sharif F (2012) J Appl Polym Sci 125:E435
32. Afshar A, Hosseini MS, Behzadfar E (2014) Sci Iran Trans C 21:2107
33. Hajibaba A, Naderi G, Esmizadeh E, Ghoreishy MHR (2014) J Compos Mater 48:131
34. Esmizadeh E, Naderi G, Bakhshandeh GR, Fasaie MR, Ahmadi S (2017) Polym Sci Ser B 59:362
35. Wang Y, Chen F-B, Li Y-C, Wu K-C (2004) Compos B Eng 35:111
36. Esmizadeh E, Naderi G, Ghoreishy MHR (2013) J Appl Polym Sci 130:3229
37. Paran S, Naderi G, Ghoreishy M (2017) Polym Compos 38:E451
38. Taghizadeh E, Naderi G, Razavi-Nouri M (2011) Polym Test 30:327
39. Dadbin S, Noferesti M, Frounchi M (2008) Macromol Symp 274:22
40. Coppola S, Balzano L, Gioffredi E, Maffettone PL, Grizzuti N (2004) Polymer 45:3249
41. Nematollahi M, Jalali-Arani A, Modarress H (2019) Polym Int 68:439
42. Mohan T, Kuriakose J, Kanny K (2011) J Ind Eng Chem 17:264
43. Andideh M, Naderi G, Ghoreishy MHR, Soltani S (2013) Polym Plast Technol Eng 52:1016
44. Razak JA, Ahmad SH, Ratnam CT, Mahamood MA, Mohamad N (2015) J Mater Sci 50:6365
45. Julie Chandra CS, Bipinbal PK, Sunil KN (2017) Polym Test 60:187
46. Katbab A, Nazockdast H, Bazgir S (2000) J Appl Polym Sci 75:1127

Affiliations

Elnaz Esmizadeh[1] · Taha Sadeghi[2] · Ali Vahidifar[1,3] · Ghasem Naderi[2,4] · Mir Hamid Reza Ghoreishy[2] · Seyed Mohammad Reza Paran[2]

[1] Faculty of Engineering, Department of Polymer Science and Engineering, University of Bonab, 5551761167 Bonab, Iran

[2] Department of Polymer Processing, Iran Polymer and Petrochemical Institute, 14965/115 Tehran, Iran

[3] Department of Chemical Engineering, Laval University, Quebec G1V 0A6, Canada

[4] Department of Chemical Engineering, Center for Applied Research on Polymers and Composites, CREPEC, Ecole Polytechnique de Montreal, Montreal, Canada